DESIGN OF A MULTI-SPOOL, HIGH-SPEED, COUNTER-ROTATING, ASPIRATED COMPRESSOR

by

JEFFREY H. FREEDMAN

B.S. Aeronautical Engineering
United States Air Force Academy, 1998

Submitted to the Department of Aeronautics and Astronautics
in partial fulfillment of the requirements for the degree of

MASTER OF SCIENCE IN AERONAUTICS AND ASTRONAUTICS

at the

MASSACHUSETTS INSTITUTE OF TECHNOLOGY

June 2000

Author: _____
Department of Aeronautics and Astronautics
April 13, 2000

Certified by: _____
Professor Jack L. Kerrebrock
Professor of Aeronautics and Astronautics
Thesis Supervisor

Accepted by: _____
Professor Nesbitt W. Hagood
Associate Professor of Aeronautics and Astronautics
Chairman, Departmental Graduate Committee

DESIGN OF A MULTI-SPOOL, HIGH-SPEED, COUNTER-ROTATING, ASPIRATED COMPRESSOR

by

Jeffrey H. Freedman

Submitted to the Department of Aeronautics and Astronautics
in partial fulfillment of the requirements for the degree of
Master of Science in Aeronautics and Astronautics

ABSTRACT

The current motivators in gas turbine aircraft engine design are improved efficiency and reduced engine weight. The drive for improved efficiency leads to high pressure ratio compressors with multiple stages, as thermodynamic efficiency increases with pressure ratio. These compressors are both heavy and expensive. Recent work by Kerrebrock, Merchant, and Schuler, has led to the possibility of achieving high pressure ratios with a reduction in the number of stages. These compressors use aspiration, or suction on the surface of the blades and end-walls, to keep the boundary layer attached under higher loading conditions, reducing losses. The work done by a rotor is related to the change in swirl across the blade and the rotational velocity of the blades. Counter-rotation provides for the largest change in swirl across a series of rotors, facilitating the largest pressure ratio.

A three-stage, counter-rotating, compressor was designed to take advantage of these benefits. The tip speeds were kept as high as possible to increase the work done on the flow. The final design has a three-stage pressure ratio of 27, much higher than is currently available in three stages. The blade aspect ratios are smaller than on current compressors because of the large swirl change across each blade row. The flow passage has large contractions across each blade row, causing sharper turns in the flow path than is currently observed. The design consists of the flow passage, blade numbers and locations, rotor speeds, and desired swirl changes through each blade row. These data will allow later efforts to design the blade shapes. A mean line analysis was conducted to design a three stage turbine to drive the compressor. The benefits of counter-rotation are apparent in the turbine, as the turbine is designed without inter-rotor nozzles. Reduced engine weight and improved efficiency are available through the turbine section with the elimination of these nozzles

Thesis supervisor: Jack L. Kerrebrock
Title: Professor of Aeronautics and Astronautics

Acknowledgements

I would first like to thank my parents and my grandfather for the inspiration, motivation, and support that has gotten me to this point, and helped me through a lot of hard times. I would also like to thank Katie for putting up with me this past year.

I would like to thank everyone in the lab, from professor Kerrebrock, my advisor, to Victor in the shop who I talk to when I need to get my mind out of theoretical and back to practical, to the guys in the lab who just let me ramble when I need to. I would like to thank Keith for his help on Matlab, and Yang for putting up with my asking questions all the time.

I would like to thank the staff of the sailing pavilion and the members of the Sloan crew team. It is a shame that more people do not take advantage of these two great opportunities, and more, in Boston.

Contents

List of Figures

List of Tables

Nomenclature

Roman

D	Diffusion factor
P	Pressure
T	Temperature
V	Total velocity
c	Chord
e	Polytropic efficiency
f	Fuel fraction
r	Radius
s	Spacing between blades
v	Swirl velocity
w	Axial component of velocity

Greek

ω	Rotational speed
π	Pressure ratio
τ	Temperature ratio
β	Angle between flow velocity and axial direction
β'	Angle between relative flow velocity and axial
σ	Solidity
η	Efficiency

γ	Ratio of specific heats

Subscripts

b	Denotes entering a blade row
c	Denotes leaving a blade row

Other useful notations

BLISK	Bladed disk
EGV	Exit guide vanes
HPC	High pressure compressor
HPT	High pressure turbine
IGV	Inlet guide vanes
LPC	Low pressure compressor (fan)
LPT	Low pressure turbine
PR	Pressure ratio
TE	Trailing edge
TIT	Turbine inlet temperature
TSFC	Thrust specific fuel consumption
m/s	Meters per second

Chapter 1 : Introduction

The increase of efficiency gained in the Brayton cycle brought about by increased pressure ratio is the driving force in compressor pressure ratios. Currently gas turbine engines, which operate on the Brayton cycle, employ multiple stages to achieve high pressure-ratios. Each stage adds increased weight, cost and length to the complete engine, all of which are detrimental to aircraft performance. A multi-stage, high speed, counter-rotating compressor may be able to decrease the large weight penalty associated with high compression ratios. Blades employing aspiration will decrease both the length of the compressor and the number of blades/disks. The compressor is driven by the need for a high pressure ratio with the desire to eliminate as many blade rows as possible. It is the goal of this research to do the preliminary design for such a compressor. A primary objective of this goal was to minimize the number of blade rows in a high pressure ratio gas generator. The compressor design consists of the flow passage, blade numbers and locations, rotor speeds, and desired swirl changes through each blade row. These data will allow later research to design the blade shapes as outlined by Merchant[1].

For kinematically similar flows, temperature rise scales with tip speed squared, so a high tip speed is desirable for a high temperature or pressure ratio. For the purpose of this design, the tip speed was initially 500 m/s and was subsequently decreased on some stages for structural integrity of the disks and other design considerations. The motivation behind the entire design is the development of aspirated compressors. The aspirated compressor uses boundary layer control on the blades and endwalls, allowing an increase in the amount of work done by each blade row at a given loss level. Keeping the flow attached longer and minimizing the wakes results in lower losses. This study relies upon the research done by Merchant[2], whose design removes a portion of the blade boundary layer at a critical location just downstream of the shock location. Suction

causes the boundary layer to remain attached further downstream on the blade. Aspiration allows for a blade row to function at a high diffusion factor (0.79) with the viscous losses of a blade operating closer to a diffusion factor of 0.5. Diffusion factor is a measure of the turning done by a blade and is defined by equation 1.1a

$$D = 1 - \frac{V_c}{V_b} + \frac{|v_c - v_b|}{2\sigma V_b} \tag{1.1a}$$

where σ is the solidity.

$$\sigma = \frac{c}{s} \tag{1.1b}$$

Recent computational results have shown that this aspiration goal can be achieved with a minimal amount of bleed air per stage (.5% at 1.5 PR and 2% at 3.5 PR) and experiments are currently underway to verify this analysis[3].

The compressor resulting from the analysis presented in this paper is shown in figure 1.1. The compressor is composed of three counter-rotating, aspirated stages and has a pressure ratio of 27. This design is further expounded upon in section 2.2.

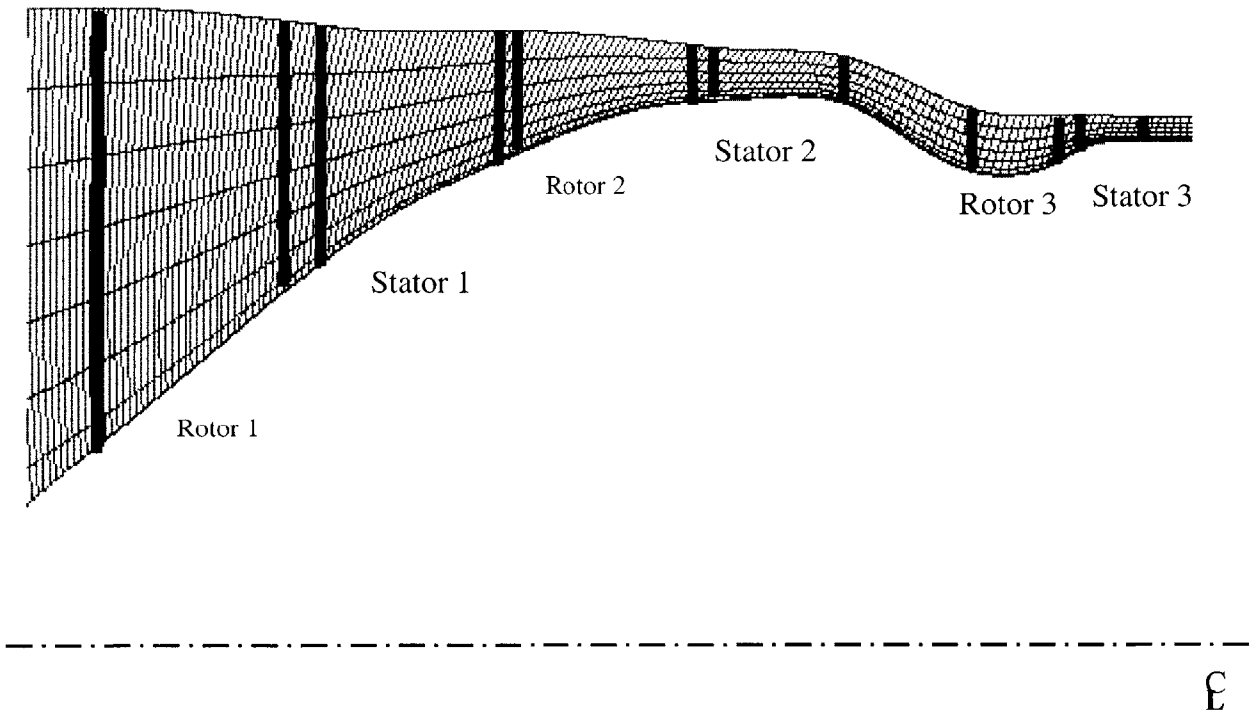

Figure 1.1 Final Design Cross Section

The design was brought to fruition in two phases. The first phase employed stream tube analysis at various span wise locations. This preliminary phase allowed for design and analysis of various compressor configurations. The second phase of design involved a CFD axis-symmetric solver to refine the design from the stream tube analysis. This phase of the design is also the first step in the iterative blade design outlined by Merchant[4]. The results of this analysis led to considerable smoothing of the flow path and lengthening of the axial projection of the blades.

1.1 Previous research

A good background discussion of previous work with compressor boundary layer control and high pressure ratio compressors is available in Design and Analysis of Aspirated compressor stages[5], Merchant. The important background to this project is research performed by Merchant who developed a methodology for the design of aspirated compressor stages.

Merchant pioneered a new methodology for the design of aspirated compressor stages, permitting improved performance that was not previously possible. The design methodology involves an iterative procedure between through-flow codes and a quasi three-dimensional viscous code with inverse design capability. Three dimensional Euler and Navier-Stokes calculations were carried out to validate the designs and experimental testing is currently underway on one of the two compressors designed in this manner.

Merchant designed both a high speed, and a low speed compressor. The low-speed compressor has a tip speed of 750 ft/s and a design pressure ratio of 1.6. Schuler is currently testing this design at the MIT blow-down compressor facility. Results have not yet been published, but data compare favorably with the computational predictions. The high-speed stage has a design pressure ratio of 3.5 at a tip speed of 1500 ft/s. This compressor is in structural design and will be tested at NASA facilities. The calculated bleed air requirement for these designs is 1% of inlet mass flow for the low-speed stage, and 4% for the high-speed stage. The results from this work lead to the choice of 0.79 for the maximum allowable diffusion factor along the blades for this work.

The compressor expounded upon in this paper can be incorporated into the design methodology used to design the other MIT aspirated compressors, and used to develop blade shapes. Data from the hub, tip, and midspan locations will be extracted and input into an inverse solver to determine blade shapes at these locations. These blades will then be stacked into a 3-D blade and the axial projection will be fed back into the throughflow

solver. This process will be repeated, and changes made to the flowpath, until convergence is reached between the two solutions. 3-D viscous codes are then used to analyze the design, and feedback is given to start the loop over again until convergence is reached between all codes.

1.2 Benefits of counter-rotation

Counter-rotation allows for a higher degree of work per stage than co-rotation, thus achieving the desired pressure ratio with fewer blades. The improvement is due to the swirl imparted in the first stage benefiting the performance of the succeeding stage. The Euler turbine equation relates the amount of work done by a rotor to the change in swirl velocity across the blade, also illustrated is the benefit of high rotational speeds.

$$C_p\left(T_{tc} - T_{tb}\right) = \omega\left(r_c v_c - r_b v_b\right) \tag{1.2}$$

A counter-rotating compressor is capable of a larger change in swirl across the blades than a conventional arrangement, with the additional prospect of eliminating the stators. This benefit comes from the fact that unlike a conventional stage, the exit swirl from the first blade row is opposite the direction of rotation of the next blade row. The counter-rotation also leads to the possibility of a drive turbine for the compressor that does not employ any stators between the separate stages. This improves the overall efficiency of the engine since less cooling air is required, and reduces weight.

Chapter 2 : Compressor Design and Analysis

The compressor design carried out for this thesis is divided into two phases. The first part of the design involved a stream tube analysis, which allowed for a preliminary method to design, and gage, various configurations. This analysis was used to determine the number of blade rows, number of spools, and the direction of rotation of the spools. The tip speed of the various rotors was also analyzed and adjusted based on a stress analysis of the disks conducted at this phase. The final configuration from this analysis was then represented in an axis-symmetric through-flow solver. This analysis elucidated aspects that were not considered in the stream tube study and led to various changes. The main change was to smooth the flow path. The requirement for a smoother flow path forced a reduction in the overall pressure ratio. The modeling provides a design that can be used to create the blade shapes, and in turn, the final aerodynamic design of the compressor.

2.1 Preliminary analysis

The main method employed for this phase involved a stream tube analysis across the blades and passages. Velocity changes across the blade were used to determine the static temperature rise. This analysis was then modified to account for both viscous and shock losses across the blades. Contractions through the flow passage were based on the continuity equation; the flow path was varied radially for smoothness. This variation minimized shock losses, and decreased the tip radius of the later stages. The radial variation also increased the aspect ratio, and decreased the required number, of blades. The final element of the design analyzed the structure and involved designing first-order bladed disks for the geometries, temperatures, and rotational velocities desired. This was necessary to insure the manufacturability of components.

Temperature rise across a rotor, given changes in flow velocities, was computed using another form of the Euler turbine equation (equation 1.2), equation 2.1

$$\frac{T_{tc}}{T_{tb}} - 1 = \frac{(\omega r_c)^2}{C_p T_{tb}} \left[1 - \frac{w_c}{\omega r_c} \left(Tan\beta'_c + \frac{w_b}{w_c} \frac{r_b}{r_c} Tan\beta_b \right) \right] \tag{2.1}$$

The flow path was computed at the tip, hub, and mean area streamline of the core flow and at the tip and hub streamline for the bypass flow (in cases analyzed with a bypass). The amount of work done by each stage is limited by the maximum allowable diffusion factor: for this analysis D_{max}=0.79. A limiting diffusion factor was chosen from results of previous research and expected efficiency[6]. Viscous and shock losses were computed for the stages to modify the ideal pressure rise associated with the calculated temperature rise. Viscous losses have a direct relationship to the diffusion factor, which is given by equation 2.2.

$$\overline{\omega}_b \left(\frac{Cos\beta_c}{\sigma} \right) \left(\frac{Cos\beta_c}{Cos\beta_b} \right)^2 = f(D) \tag{2.2}$$

Assuming viscous losses corresponding to a diffusion factor of D=0.5, the value for f(D) was retrieved from empirical charts[7] and used to calculate the loss parameter. The viscous losses of the rotor were computed using equation 2.3 after the loss parameter was calculated.

$$\eta_s \approx 1 - \frac{1}{2}(\gamma - 1)\overline{\omega}_b \tag{2.3}$$

The final losses included, shock losses, were computed assuming a pressure drop corresponding to a normal shock at the blade's relative Mach number. This method gave a higher loss than we would hope to achieve, but was a conservative starting point for a design iteration.

The large pressure changes across the blade rows necessitated an area change that was larger than is usually seen in modern designs. Area change through the blade passages was computed using a modified form of the mass flow parameter given in equation 2.4.

$$\frac{A_2}{A_1} = \frac{P_{T1}}{P_{T2}} \sqrt{\frac{T_{T2}}{T_{T1}}} \frac{M_{x1}}{M_{x2}} \frac{\left(1 + \frac{\gamma - 1}{2} M_2^2\right)^{\frac{\gamma+1}{2(\gamma-1)}}}{\left(1 + \frac{\gamma - 1}{2} M_1^2\right)^{\frac{\gamma+1}{2(\gamma-1)}}} \qquad (M_x = \text{axial M}) \qquad (2.4)$$

Flow properties through a stage were approximated by the tip properties, assuming minimal radial variation. The radial variation on the first rotor blade shows the largest deviation from this assumption where the total temperature decreases by 4.4% from tip to hub and velocity decreases 11% from hub to tip. Static temperature was computed from the relationship between T, T_T and V. The static temperature was then used to compute the Mach number for equation 2.4.

The large contractions through the blade passages lead to a small area for the last blade row. Flow was directed either in or out radialy to create smooth flow paths while increasing the blade height of the last compressor stage. If this were not done, the blade height of the last rotor would be 2.2% of the first rotor for a compressor compression ratio of 31, as opposed to the 3% this feature generates. For a fan with a 1m diameter, the last rotor blades would be 30mm tall at the TE as opposed to 22mm, a difference of 30%. Maintaining the larger radius at the same chord would also require 1.3 times as many blades to keep the same solidity. These blades would have a smaller aspect ratio, increasing the effect of tip clearance and secondary flows. In re-directing swirled flow radially, it was important to conserve the angular momentum of the swirl velocity. No flow passage losses were computed for the initial design and the flow-path was smoothed out visually to reduce real losses. The smoothing was not done in any quantitative manner, but rather was judged by eye after a spline was fit to the points defining the flow path.

2.1.1 Compressor configuration

The configuration of the compressor, number of spools and number of blade rows, relative rotation of rotors, etc... was optimized through multiple iterations. The first step involved selecting the number of stages required to achieve a pressure ratio suitable for a core compressor on a next generation high pressure ratio engine, or an engine comparable to modern military engines. Each stage was designed as a counter-rotational spool, allowing autonomy from the other stages. Once the appropriate number of stages was determined, the configuration of the spools, and whether the last stage should be aspirated, was studied to determine the marginal benefit of added complexity.

2.1.1.1 Evolution of the three stage design

One of the simplest designs to examine involves a compressor with inlet guide vanes, two counter-rotating rotors, and exit guide vanes. The cross section for a compressor of this type is illustrated in figure 2.1.

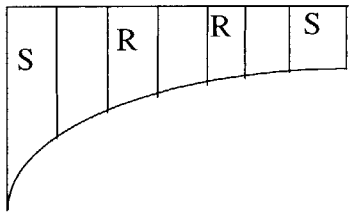

Figure 2.1 Original Counter-Rotation cross section

The inlet guide vanes imparted a swirl component to the first stage which was mirrored in the exit swirl of the first stage and into the second stage. The imparted swirl was in the opposite direction of rotation, increasing the relative Mach number. A velocity triangle diagram for this configuration is given in figure 2.2.

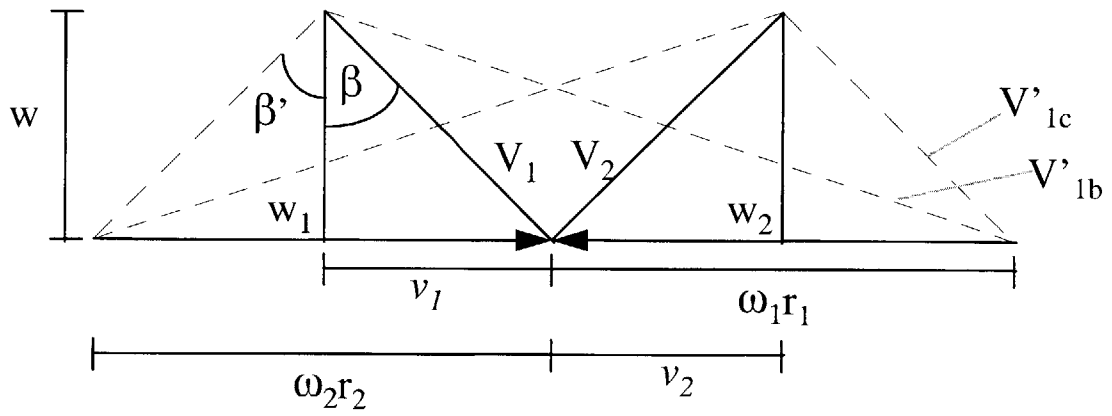

Figure 2.2 Design starting point velocity triangles

One of the benefits of this design was that the rotor blades would be nearly mirror images of each other, simplifying the aerodynamic design process. From initial estimates, a pressure ratio over 20 would be possible from this design. Such a compressor used behind a fan, or on its own, would be able to revolutionize both engine and aircraft design.

The initial design, while simple, was not practical. Inlet guide vanes were required to accelerate the flow above Mach one, requiring a convergent-divergent nozzle in the stator passage. Drawbacks of this configuration begin with, but are not limited to, the complexity of this requirement. The design was also very inefficient. With a tip speed of 500 m/s, the relative mach number of the first rotor is over 2.5. This high Mach number results in unacceptable shock losses. The relative Mach number for the second rotor is a more modest 1.6, which yields acceptable losses for this analysis where shock losses were limited to M=1.7. The limit in tip speed stems from research done on the high speed compressor designed by Merchant.[8] Large temperature rises across the first rotor decrease the incident Mach number of the second rotor.

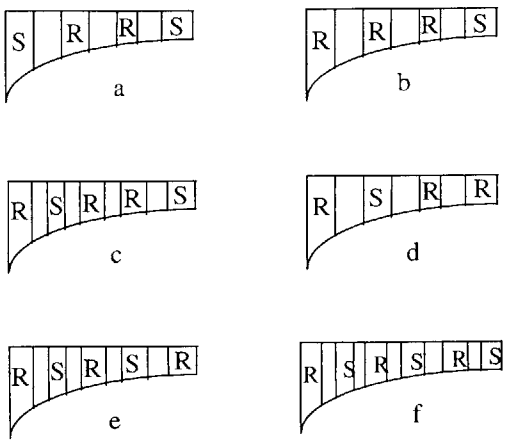

Figure 2.3 Various Compressor Configurations

The problem of the stator requiring a convergent divergent nozzle was remedied by replacing the inlet guide vanes with a third, high speed, counter-rotating, rotor; figure 2.3 (b). The first stage imparts the desired swirl magnitude to the second rotor, allowing the rest of the compressor to behave closer to original expectations. Solving the problem of the proper magnitude of swirl into the second stage resulted in little benefit on the high relative Mach number problem. The only reduction in relative Mach number stemmed from the increase in speed of sound due to the increased temperature.

The goal of minimal blading dictated that all configurations have the fewest number of stator rows possible. The exit swirl from the first rotor could be decreased, unloading the rotor and reducing the relative mach into the second row, but if this third stage was to be added, it should be loaded to the maximum allowable by aspiration. The design requirement of loading the first rotor as high as possible dictated the addition of a stator to reduce the inlet mach number of the second stage. The result of this stator addition is illustrated in figure 2.3 (c).

A rotor with the desired inlet swirl of the initial concept, and low losses, was deemed unobtainable. The second rotor was able to achieve a much higher compression ratio

with the stator because of reduced shock losses. Relative Mach, and the induced shock, was decreased from on the order of M=2.5 down to M=1.7. This reduction translates to a pressure ratio across the shock of 0.5 up to 0.86. An important note is that while there was a stator introduced at this point, the stator did not take away from the benefits of counter-rotation. The stator reduced the amount of exit swirl, but did not turn the flow through the axial direction. If this relative velocity were required in a synchronous-rotation design, the solidity of the stator would be much higher, requiring an increased number of blades. The final design from this phase yields a solidity at the tip is 0.68, requiring 47 blades, with a diffusion factor of 0.69

The investigator was still optimistic about the possible success of the last two rotors operating as originally envisioned, without a stator in between them, one benefiting from the exit swirl of the other. The problem was that if the second rotor was used to its maximum potential, the third rotor suffered unacceptable shock losses. A sensitivity analysis was done on the total amount of work possible out of the last two rotors based on the exit swirl out of the second rotor to maximize total pressure rise. The important result from this analysis was that at the maximized configuration, the exit swirl from the third rotor was almost negligible. The optimized configuration for the rotors left a row of exit guide vanes that were very lightly loaded, a diffusion factor of around 0.1. At this point another design was conceived that did not need exit guide vanes while operating at the design point, figure 2.3 (d).

This new design modification did not have a large effect on the compression ratio of the last rotor, and was thus adopted as another possibility in the design choices. The lack of exit guide vanes will decrease the performance of the compressor at off design conditions. Exit guide vanes would most likely be installed in an engine with a zero exit swirl design to improve performance at this condition.

The final major change in the hardware configuration of the design came as a logical progression of the other changes. A second stator was added behind the second rotor,

figure 2.3 (e) and (f), allowing the second rotor to achieve a higher pressure-ratio while decreasing the relative mach number of the third rotor. The addition of the stator adds another source of shock losses. However two normal shocks at M=1.7 are still less of a pressure loss than one normal shock at M=2, which represents the order of magnitude of this change. The velocity triangles for the mean streamline through each blade, for a compressor of the type illustrated in figure 2.3 (e), are illustrated in figure 2.4.

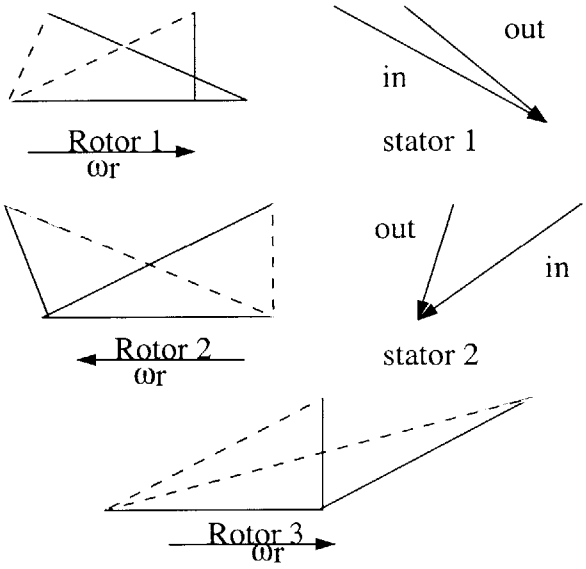

Composite velocity triangles at mean streamline

Figure 2.4 Mean line Compressor Velocity Triangles

(Stators are at different radii than rotors)

Limiting the last rotor to zero exit swirl proved important in performance when a stator was added between the second and third stages. The stator allowed both stages to become more effective. The third rotor, preceded by a stator, was capable of imparting significantly more exit swirl to the flow. Zero exit swirl severely decreased the pressure ratio the compressor was capable of. While the zero exit swirl design had a lower pressure ratio than its counterpart with EGV's, it was superior in terms of thermal efficiency. The increase in efficiency is due to having one less blade row to incur losses. A high exit swirl from the third rotor created supersonic flow over the stators, resulting in shock losses. The zero exit swirl also maintained some simplicity in reducing the blade count of the machine. However, once again the goal was a high pressure-ratio, and EGVs

will be needed for off design conditions. All these factors led to the selection of configuration (f) in figure 2.3 as the final design choice once the second phase of design begun.

2.1.2 Flow passage design

The design of the flow passages presents a significant challenge. From equation 2.1, it is desirable to have the tip radius of the rotors increase across the blade, or at least limit the decrease through the blade. Having the last rotor and stator at a low tip radius is desirable to decrease the number of blades in these rows. The spacing, for a given number of blades, is less at a smaller radius, so the chord required for the solidity will also be decreased. The lower radius will also increase the blade height, increasing the AR. A large AR will minimize the effects of tip losses and secondary flows as a percentage of through-flow. The tradeoff between increasing the tip radius of individual rotors and keeping the last stages at a low radius, was weighed against the high compression ratio of the design. The high compression ratio means that there is a large area change through the blade rows. All of these effects tend to create a convoluted flow path, necessitating a balance act between all of these driving factors.

The smoothest flow path is attainable by decreasing the tip radius of the rotors and angling the flow passages down toward the hub between the blade rows. This process lowered the compression ratio of each stage, and the area changes through the rotors were not significant. The decision to lower tip radius was also based on research that has been done on the design of aspirated compressor stages[9]. The flow path for the concept-1, the final design for this phase, is angled outward after the first rotor, decreasing the swirl through conservation of angular momentum, and decreasing the shock losses. The flow is then angled down towards the next rotor. Placing the stator at a higher radius than the rotor decreases the Mach number that the stator sees, decreasing the shock losses. The predicted efficiency for this design is higher than one where the stators are not at a higher

radius than the rotors, but only by approximately 1%. The difference in pressure ratio incurred from this change however is a greater 4% decrease. Again, it must be noted that there was no consideration given for the losses that would be incurred by traversing any of these passages. The losses in the passages were not expected to negate the benefits of this configuration.

The result of radial manipulation can be seen in the concept-1 cross section, figure 2.5. The flow path was adequate for this phase, but had problems that required a radical redesign for the next level of analysis. The design, while not incorporated into the final compressor, illustrates some aspects that would be advantageous to incorporate if possible at later points. It also illustrates the problems associated with matching several large pressure ratio compressor stages. Smaller pressure ratios allow for a more gradual decrease in tip casing, allowing the final blades to have adequate ARs.

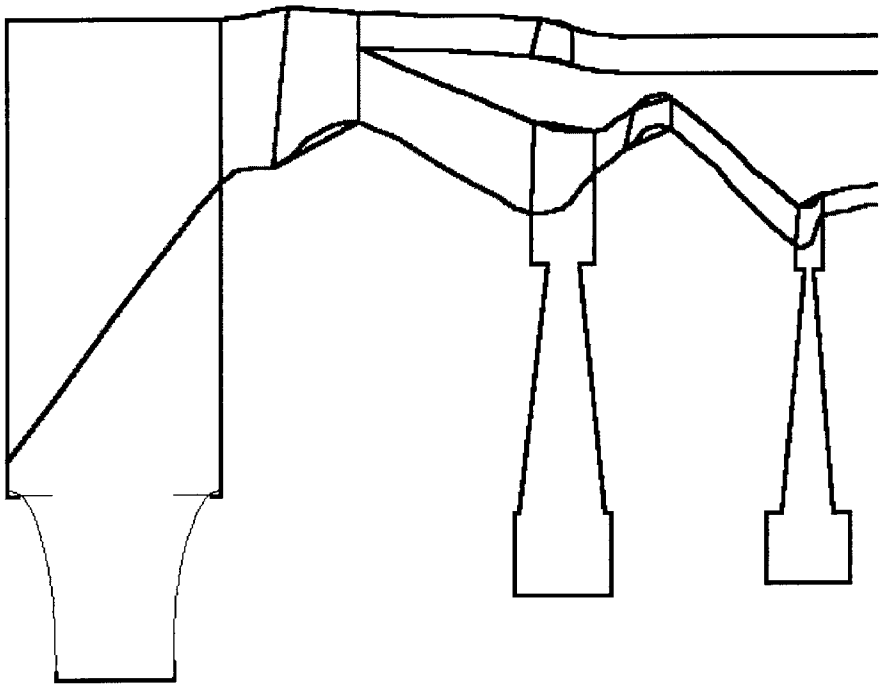

Figure 2.5 Concept-1 Cross section

2.1.3 Blisk design

The choice of a high rotational speed for the blade tips, while contributing to higher pressure ratios, is also the cause of some problems. The impact of this design choice to be dealt with here is that of stress and material selection. The stress on a blade of constant cross sectional area is given by equation 2.5.

$$\sigma = \frac{\rho\omega^2 r_T^2}{2}\left[1-\left(\frac{r_H}{r_T}\right)^2\right] \tag{2.5}$$

The BLISKs are modeled with an outer rim, where the blades are attached, a constant stress disk, and an inner rim that that holds the disk together. This design carries the load created at the rim, where the rotational speed is high, towards the center of the compressor where the rotational speed is less, and therefore the stress is also less. There are materials available for the first two stages to enable the rotor to rotate at the desired high tip speeds. The first and second rotors are both feasible in a Titanium alloy, Ti-5Al-2.5Sn. The Titanium alloy was chosen because of its strength at temperature. There is not a material available to allow for the same tip speed on the third rotor. The temperature is much higher for this rotor than the second rotor, necessitating a Nickel alloy, Inconel X, which combined with the geometry, requires a lower tip speed. The third rotor is at a much lower radius than either of the other two rotors. This means that for a given radius of the inner rim, and a given tip speed, the inner rim of the third rotor experiences a higher speed than the other two rotors with their larger tip radii, causing the associated higher stresses. It is for the combination of the higher temperatures and the smaller tip radius, that the tip speed of the last rotor was decreased from 500 m/s to 400 m/s for the concept-1. The tip speed of the last rotor was further reduced to 300 m/s for the final design since the chord was increased.

Stage	Normalized Tip Radius	Material	Temp.	Tip Speed
1	1.00	Ti-5Al-2.5Sn	438 K	500 m/s
2	0.84	Ti-5Al-2.5Sn	711 K	500 m/s
3	0.67	Inconel X	815 K	400 m/s

Table 2.1 Material and tip speed summary for concept-1 compressor

2.1.4 Concept 1 compressor design summary

The end result from this aspect of the study is a three-stage, counter-rotating compressor producing a pressure ratio of 31. The Polytropic efficiency at the tip is 87% and 91% at the hub, the difference stemming primarily from shock losses. The tip speed of the first two rotors is 500 m/s and 400 m/s at the tip of the third stage. The flow path for this design is illustrated in figure 2.5 and some important parameters are summarized in table 2.2. Additionally, the velocity triangles corresponding to the mean streamlines of the concept –1 compressor blades are given in figure 2.4 .

Table of Stage Properties						
	Rotor 1	Stator 1	Rotor 2	Stator 2	Rotor 3	Stator 2C
π	4.19	0.989	4.48	0.989	1.65	0.99
D_{max}	0.79	0.69	0.79	0.32	0.60	0.54
Blades	23	47	116	162	139	47
Mb'_{max}	1.71	1.27	1.65	1.19	1.67	0.78
Values at Mean area streamline of core flow						
$\beta b'$ (deg)	53.3	49.5	61.4	56.5	68.6	
$\beta c'$ (deg)	14.1	0.25	0.4	0.79	53.3	
relative property for stators is non-rotating frame						
				tip		hub
Adiabatic efficiency				0.794		0.864
Polytropic eficiency				0.867		0.913

Table 2.2 Concept-1 design parameters

2.2 Computational modeling

While the first stage of the design involved selecting the best configuration for the compressor, a more realistic modeling tool was necessary to further analyze the feasibility of the design. The design was also modified to use a first rotor similar to the MIT high-speed aspirated compressor stage. This stage has a pressure ratio of 3.7 at a tip speed of 457 m/s[10]. Use of this rotor will simplify design and testing of the complete compressor.

The analysis of the compressor involved representing the compressor in an axisymetric solver. The code used was MTFLO[11], written by Professor Drela at MIT, and the specifics of the code are included in Appendix A. The program requires two input files: one file includes the flow passage geometry for the compressor; while the other file contains the blades' location, rotational velocities, swirl changes, and entropy losses.

One of the limiting factors about the code was the inability to separate the flow passage into a core stream and a bypass stream. This limitation meant that the compressor would have to be analyzed with zero bypass. There was also no ability to change the mass-flow through the blade rows. In actuality, the mass flow would have to be diminished through each blade row to represent the aspiration of the boundary layer.

2.2.1 Methodology

The starting point for this analysis was a modified version of the concept-1 compressor which used aspiration in the third stage to help counter the loss of pressure rise in the downgraded first stage. The flow paths from the initial analysis were also found to be too serpentine, causing massive flow separation in the passages, and were smoothed out. The smoothing of the flow path increased the radius and chord of the last rotor, requiring a

reduction of tip speed to 300 m/s for structural feasibility. A pressure ratio of 41 was thought to be possible with three aspirated stages and three sets of stators.

In the previous section, the cross sections of the compressors analyzed had high aspect ratio blades. The blade chord was kept low, creating blades that looked similar in dimension to current compressors when the flow path is viewed in cross section. The large turning done by the blade rows was found to necessitate a longer axial distance across each blade row. The initial geometries analyzed did not incorporate this, and the large velocity change in the short distance was causing high Mach number excursions through the blade rows. These narrow blades, and their requested work input, were causing code convergence problems. Physically, this is logical because if the desired solidity were to be achieved using high AR blades, each blade would have a very sharp curve in them that the flow would not be able to easily follow. Lengthening the chord of the blade makes the velocity change more gradual. An important note from this is that the diffusion factor, which incorporates only solidity, does not fully cover the loss correlation. A relationship between the tangential velocity change across a blade and the chord of the blade is also necessary to gage if a design is within a good design limit.

Another major change in the designs is that the pressure ratio across the blades is lower than in the stream tube analysis. The CFD model of the compressor computed higher diffusion factors for the blade rows than the stream tube analysis. This higher diffusion factor meant that the pressure ratios across the blades had to be lowered. While the compressor was changing because of the analysis of the CFD code, the results were put back into the original model to help determine the swirl changes necessary through the stators. While is was an obvious decision to change the swirl through a rotor and make it lower if the diffusion factor is too high, it is not as obvious as to what the best swirl condition for the next rotor would be. The quickness of the stream tube analysis was very useful here for those changes.

The solver did not have a loss function for shock losses, it conducted a simple viscid analysis. The entropy loss across the expected shocks was input as condition along the blade rows. The entropy loss across the rotors was adjusted so that the polytropic efficiency was between 94- 95%. The stators were also charged with losses, and adjusted so that the overall polytropic efficiency of the compressor is ~90%. Losses will be analyzed in more depth when the blade rows are studied and designed. Those losses can then be input back into this model and the model adjusted. Blade design is beyond the scope of this thesis.

2.2.2 Final Compressor

The result of this analysis is a three-spool, counter-rotating compressor that employs aspiration on all 6 blade rows. The overall stagnation pressure ratio for this design is a little over 27, while, by assumption, the overall polytropic efficiency of the compressor is ~90%.

Table 2.3 summarizes the properties through the final compressor section illustrated in figure 2.6. The total pressure rise through the compressor is almost constant radially, while the static pressure rise is slightly larger at the tip, as illustrated in figure 2.7. The diffusion factor of rotor 1 peaks near the tip, while the diffusion factors of rotors 2 and 3 are more constant and closer to the limit. Radial variations of blade properties decrease axialy through the compressor as the difference between hub and tip speeds decrease in the rotors. This trend is visible in both figure 2.8 and figure 2.9 which plot the radial variation of properties for each blade row. As an aid in understanding the velocity changes through the blade rows, the mean line velocity triangles for this design are given in figure 2.10 while figure 2.11 has single arc representations of blade shapes corresponding to these velocity changes.

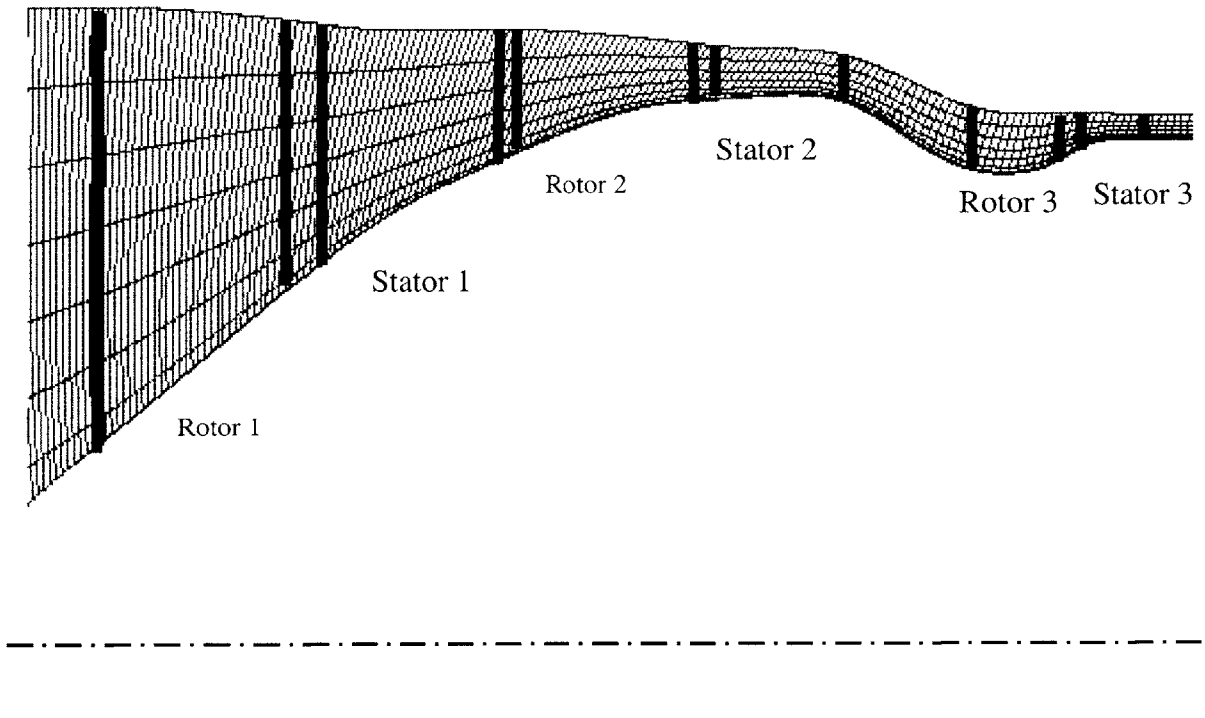

Figure 2.6: Cross section of compressor

	Tip speed	Π	# Of Blades	D_{max}	Normalized Tip Radius
Rotor 1	**475 m/s**	**3.59**	**33**	**0.733**	**1.000**
Stator 1	**0**	**0.93**	**25**	**0.724**	**0.967**
Rotor 2	**512 m/s**	**3.93**	**27**	**0.713**	**0.961**
Stator 2	**0**	**0.95**	**17**	**0.679**	**0.936**
Rotor 3	**313 m/s**	**2.29**	**63**	**0.763**	**0.839**
Stator 3	**0**	**0.95**	**79**	**0.639**	**0.836**

Table 2.3 :Table of blade properties

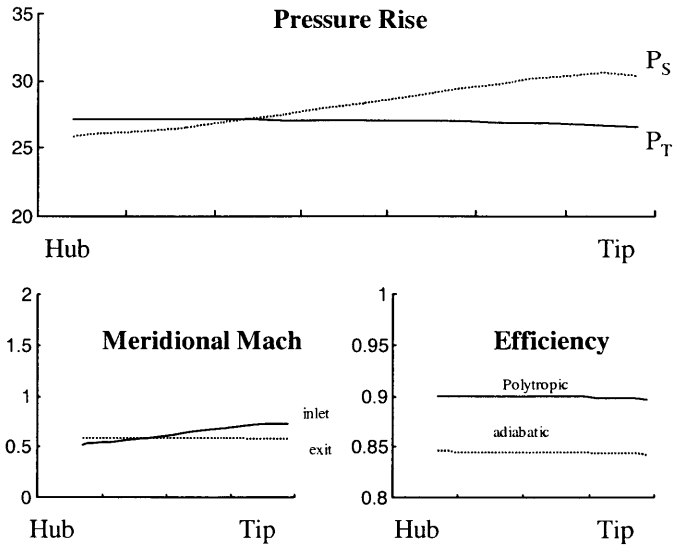

Figure 2.7: Qualities across the entire compressor

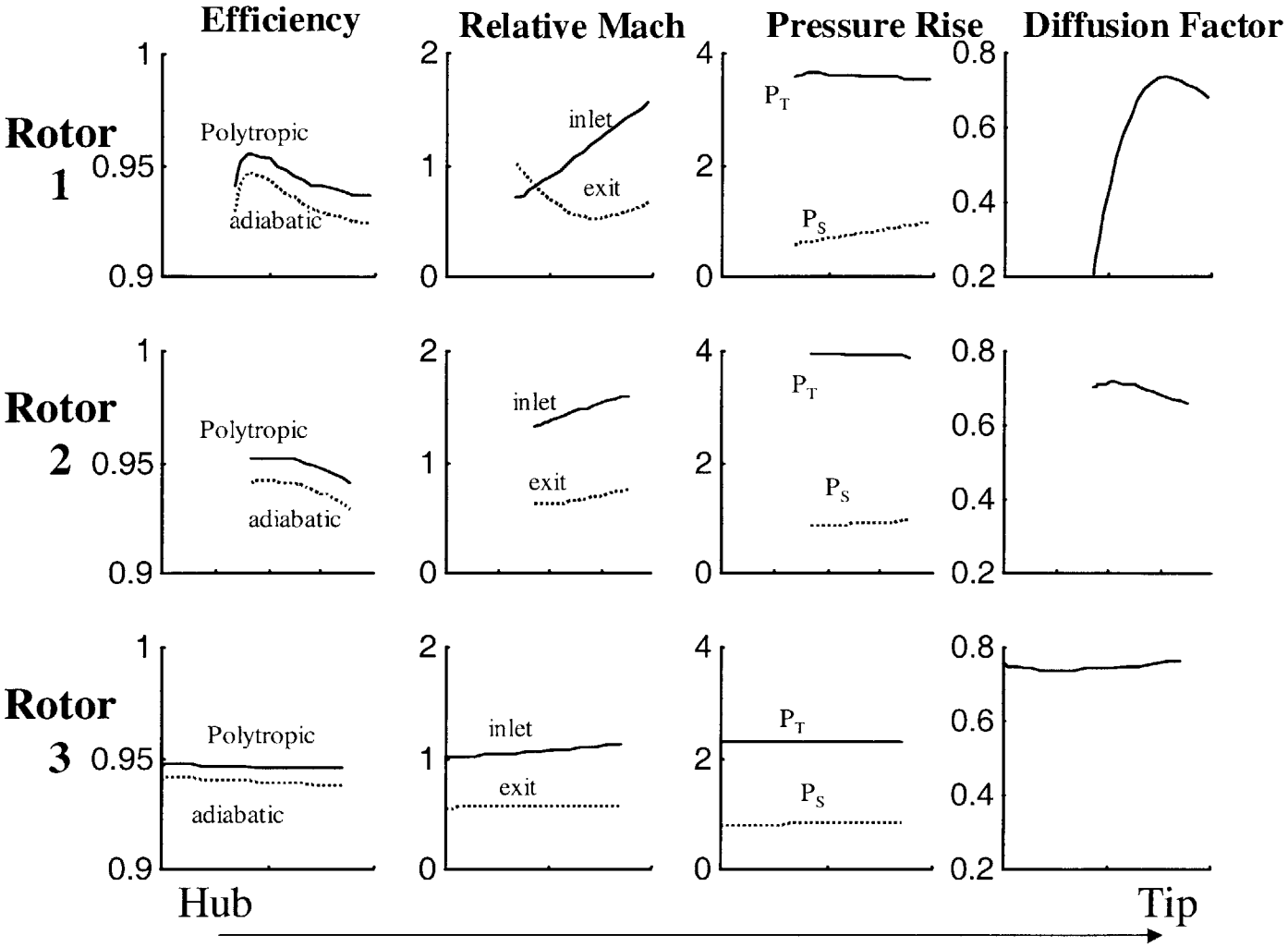

Figure 2.8: Qualities across the rotors

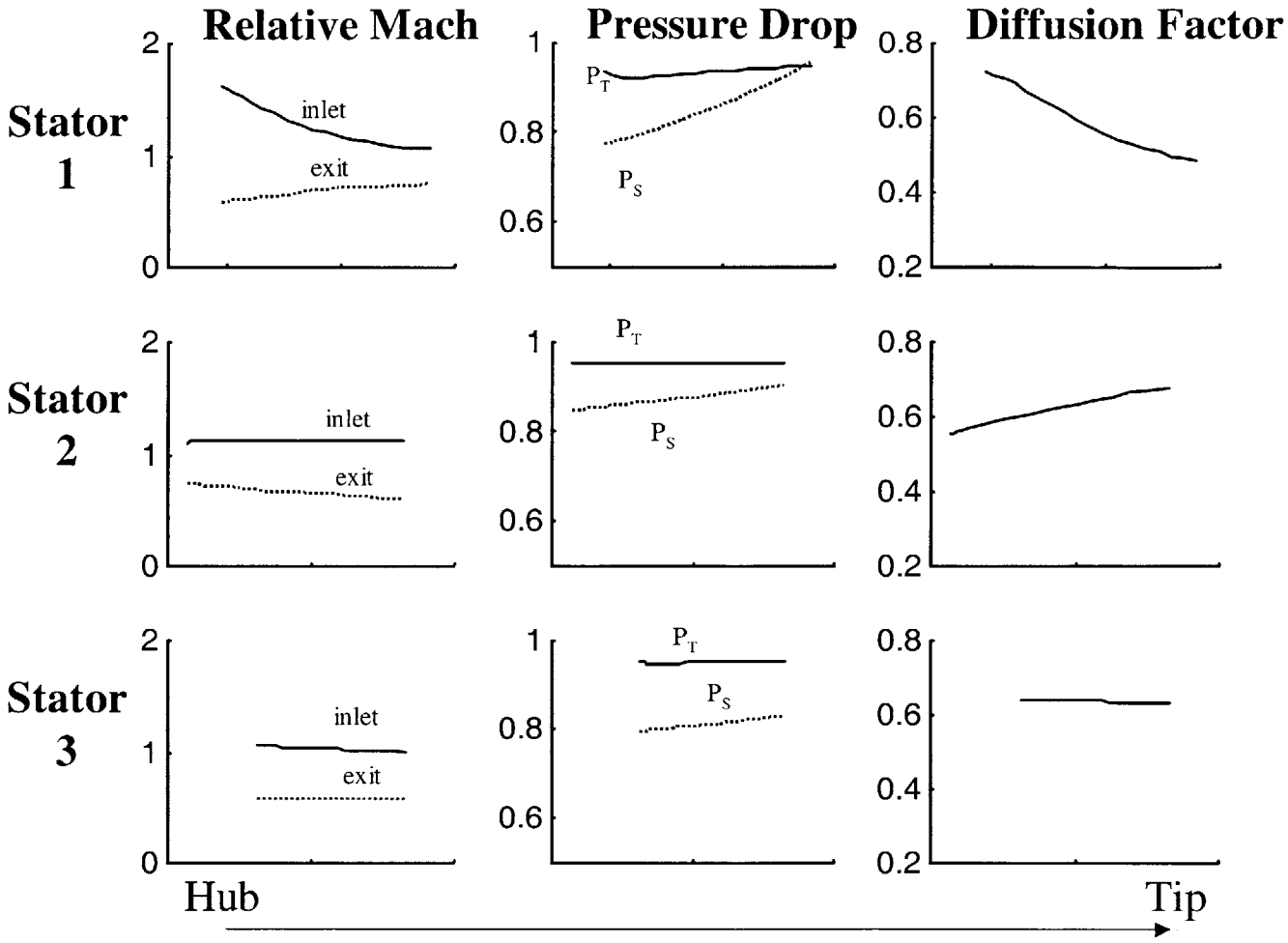

Figure 2.9: Qualities across the stators

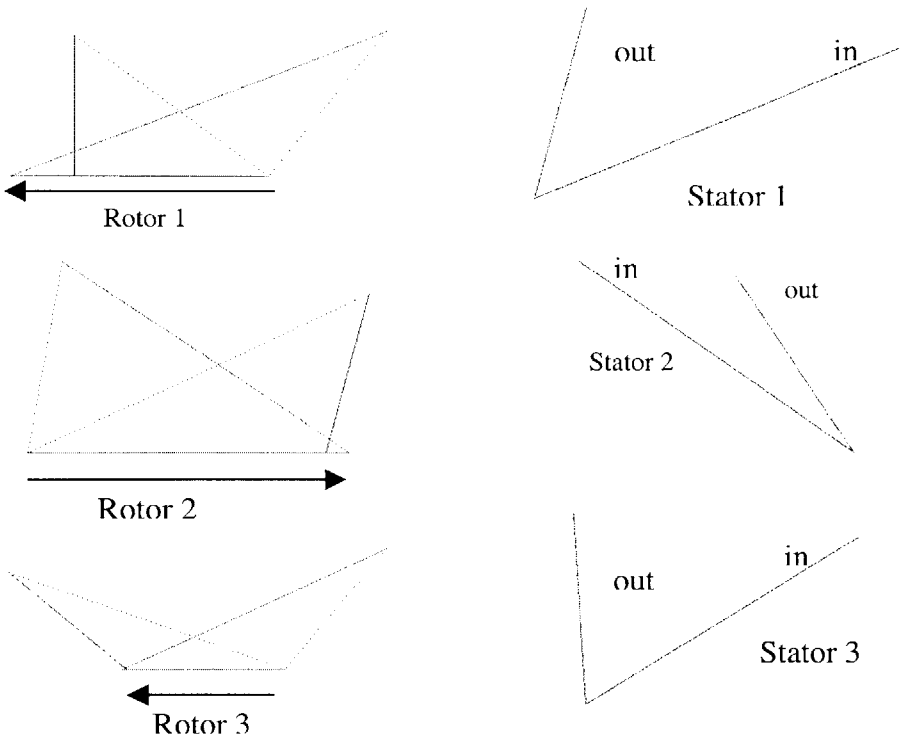

Figure 2.10: Compressor velocity triangles at mid-span

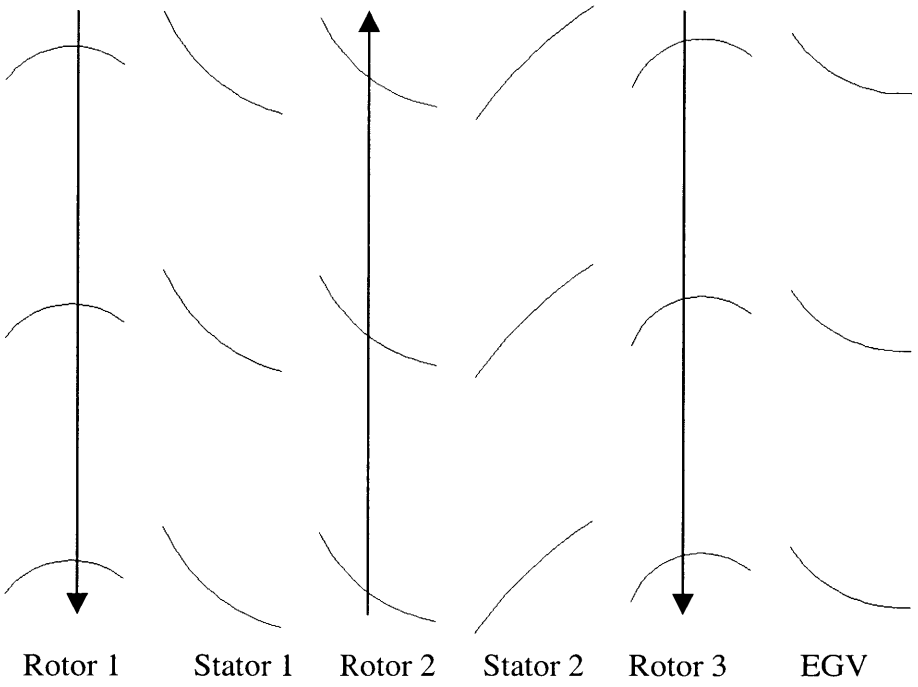

Figure 2.11: Compressor blade shapes at mid span

Chapter 3 : Combustor and Turbine Design

The compressor must be matched with the other components of an engine to achieve functionality. The overall goal of the project is to asses the applicability of aspiration technology. To this end a combustor design and a mean line turbine design were conducted to match the aspirated compressor. This three stage turbine was designed to utilize the benefits of counter-rotation and minimize the blade rows in the turbine. This overall design could be used as the gas generator in an application where a fan supercharges the first rotor and is driven using a gearbox. In this instance, it would only be necessary to add some turbine stages to the end of the LPT.

3.1 Combustor Design

The design of the combustor assumes a 10% bleed from the compressor core flow even though the compressor design does not account for this bleed. The change for the compressor will come when a more detailed analysis is done on the requirements for the aspiration. The bleed air may not all be from the aspiration, but this is an estimate as to the amount of air that will be needed for the cooling of the turbine. The fuel flow is designed to raise the core flow to the desired turbine inlet temperature of 1900^0K.

The first step in the burner was to determine the amount of fuel relative to air that would be necessary for the burner to achieve the desired exit temperature. The fuel to air ratio in the combustor is 0.036 assuming standard kerosene as the fuel, yielding an equivalence ratio for the mixture that is well below the acceptable limits for combustor stability. This low equivalence ratio is expected and is the reason all modern burners have primary combustion zones. The primary combustion zone of this combustor is sized so that the equivalence ratio in this zone will be unity at SLS conditions.

The flow exiting the compressor is traveling at speeds far to fast for efficient combustion, on the order of M=0.58. It is necessary to slow the flow down so that combustion can occur, and be completed, in a relatively short length before the flow enters the turbine. The maximum area of the burner is sized to accommodate the flow moving at 30m/s prior to entering the primary combustion zone. To slow the flow from the high compressor exit Mach number, the standard arrangement of a two-part diffuser is utilized.

The first part is a straight diffuser, which then empties into a dump diffuser to attain the desired flow velocities. The two part diffuser is used as a compromise between combustor size and combustor pressure loss. A straight diffuser would be too long, while a dump diffuser would be short, but would have an unacceptable pressure loss. The net pressure drop caused by these two diffusers is 4.78% loss. The length of the combustion chamber is scaled from the F100 engine to facilitate the proper residence time, and does not change based on the size of the engine. The required length of a combustion zone is directly related to the exit pressure from the compressor and the turbine inlet temperature. The F100 was used to scale the appropriate length because of the similar pressure ratio and it employs modern technology. The scaling of the combustor length is accomplished using equation 3.1, where the constant is taken from the F100.

$$L \propto P_{t3}^{-.714} / \sqrt{T_{t4}} \tag{3.1}$$

The liner cooling flow, and the remaining core flow, is split equally between the inner and outer sides of the burner. The liner cooling flow is necessary to maintain structural integrity in the burner. The precise method of cooling the combustor walls has not been decided. It is likely the design would incorporate a standard impingement cooling design, but the new transpiration cooled combustors would be even better. The choice of fuel nozzles, and their number, has not been made at this stage. A diagram of the combustor is given later in figure 3.3.

3.2 Turbine Design

A goal for the turbine design, similar to that of the compressor design, is to minimize the number of stages. The design of the turbines employs no new technology or special concepts. The turbines are designed to take advantage of the counter-rotation to eliminate the stators typically found before each turbine rotor. This design will save cooling air and shorten the length of the engine. A three stage turbine was designed to power the modified compressor and has two rows of guide vanes. One set of guide vanes is the nozzle at the inlet to the turbine, while the other set straightens the flow from the last rotor.

Blade cooling analysis was not conducted for the design of the blades, however there is an allotment for cooling air that has been taken out of the turbine flow. The high-pressure spool is debited 10% of the core flow for the first stage and 5% for the second stage, while the low-pressure spool has a debit of 0%. A correction to these assumptions will obviously be made once the correct amount of cooling flow has been determined. These assumptions are of consequence, however they are of the correct order of magnitude for this type of design.

The blade cooling air will be coming from various stages of the compressor, however there are no numbers available at this stage of the design for the required bleed air from each stage. For the purpose of the power balance, each aspirated stage was debited ~3% of the air that goes through it. No temperature or pressure change was calculated at each turbine stage for the addition of cooling flow. The assumption in the design is that the following stage will see the exit conditions of the previous with the exception of an increase in mass flow from the previous stage's cooling air. This is not an accurate assumption, but is close enough for the preliminary study. The additional flow is small and the pressure can be matched closely for some of the stages. The methods for physically dealing with the compressor bleed, and aspiration, have not been addressed in this study.

The design of the turbine is not as thorough as the design of the compressor, as it was not a principal goal of this project. A mean line analysis was conducted to design an appropriate turbine. The major factor that was detrimental to the design of the turbine was the slow rotational speed of the first turbine. The high temperature, and large radius of the compressor limits the rotational velocity of this turbine stage. The low rotational speed of the first rotor, coupled with the work requirement, dictates a inlet nozzle that is not choked. The result of the design is a three stage turbine without any intermediate nozzles.

Turbine losses and loading was analyzed using a correlation between the stage loading parameter, equation 3.2, and the flow coefficient, equation 3.3.[12]

$$\psi = \frac{C_P \Delta T}{(\omega r)^2} \tag{3.2}$$

$$\phi = \frac{V_{axial}}{\omega r} \tag{3.3}$$

Predicted efficiencies for the turbine stages, as well as their loading and flow coefficients is included in table 3.1. Another method for judging the stage loading and loss, similar to the diffusion factor in compressors, is the Zweifel coefficient. One method of choosing turbine solidity is based on this coefficient, and optimal efficiency is in the range of ψ_z=0.8-1.0 for a wide range of designs.[13] A simple form of the Zweifel coefficient is given in equation 3.4.

$$\psi_Z = \left(\frac{v_1}{v_2} - 1 \right) Sin(2\beta_2) \frac{s}{c} \tag{3.4}$$

Velocity triangles for the turbine are presented in figure 3.1 and single arc representations of the blade shapes are presented in figure 3.2. Figure 3.3 is a representation of a counter-rotating aspirated engine with an inlet diameter sized to match a F100 engine. A representation of the F100 is presented in the figure to compare overall length as well as the reduction in the number of compressor blades and the reduced compressor length.

	Flow Coefficient ϕ	Loading Coefficient ψ	Efficiency η_{stage}	Zweifel Coeficient ψ_z(c/s)	Disk Material
Inlet Nozzle				0.96	NA
HPT 1	2.25	1.05	90%	2.53	InconelX
HPT 2	1.18	0.94	91%	1.82	IMI 680
LPT	1.04	1.01	90%	1.67	IMI 680
Exit nozzle				0 / NA	NA

Table 3.1 Turbine properties

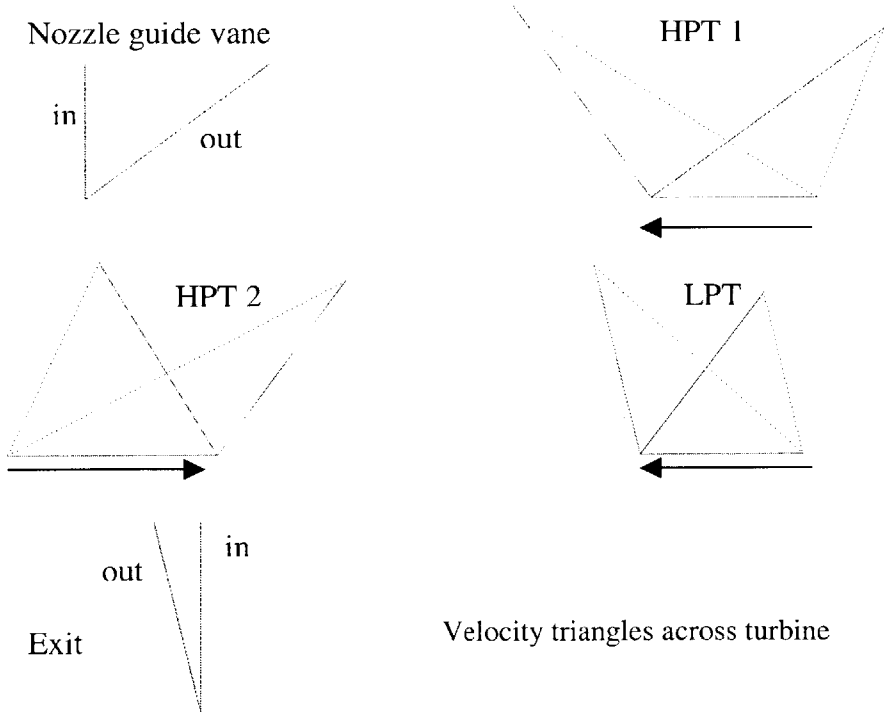

Figure 3.1: Turbine velocity triangles

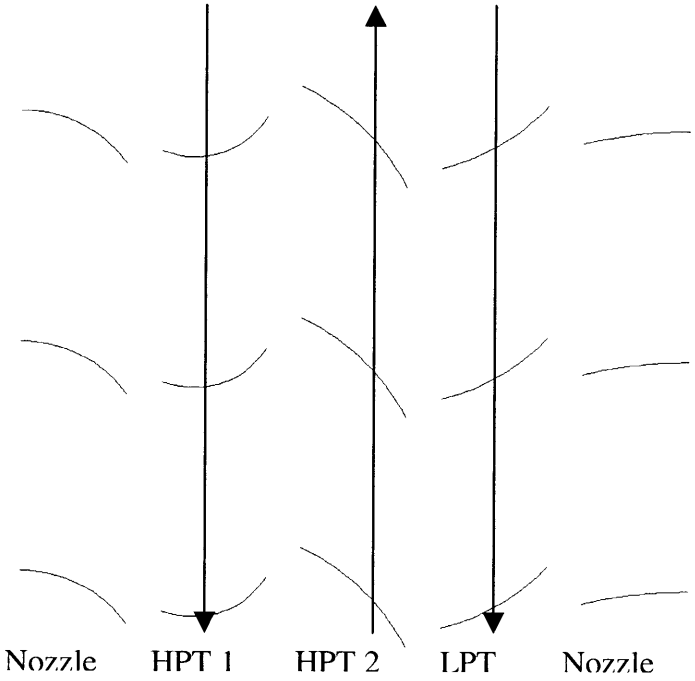

Figure 3.2: Turbine blade shapes

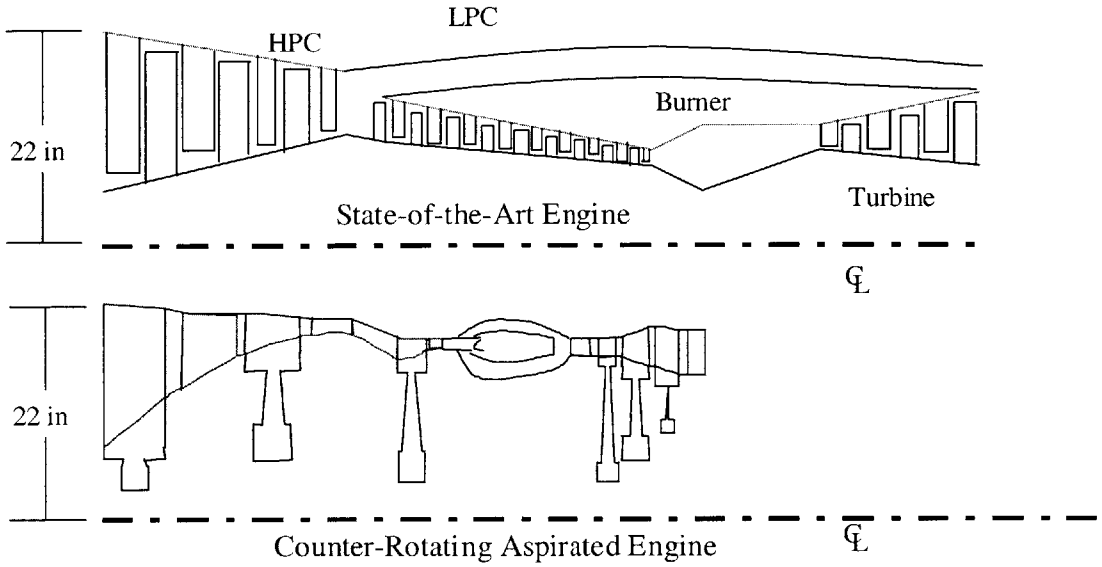

Figure 3.3: Comparison of counter-rotating aspirated engine to a modern engine

Chapter 4 : Conclusions

4.1 Summary of work

The work contained in this thesis has led to a preliminary design for a compressor that achieves a pressure ratio of 27 in three stages. The results of this design can be used as a starting point for the aerodynamic design of the blades, and the eventual structural design of the disks. The counter rotation of the spools, and the requirement for three spools, leads to a design that is complex both structurally and aerodynamically. The benefit of this complexity is the promise of a low weight engine. The engine will save weight by the elimination of multiple disks that current technology compressors require along with their multiple rotating blade rows.

A mean line design of a power turbine for this compressor has also been accomplished. This analysis shows that it should be possible to power this compressor without the need for vanes between the rotors. The Turbine section will save weight with the elimination of these nozzles, and the elimination of these nozzles will also increase overall engine efficiency by lowering the cooling air requirement. These aspects leave great promise for the next generation of aircraft engines.

4.2 Recommendations

It is necessary to design the aerodynamic blade shapes for the compressor section and determine the bleed air requirements. Once the blade shapes are designed, a structural design of the compressor disks is necessary to assess the feasibility of the concept. An important factor in analyzing the overall compressor and engine design is the bleed air required for aspiration. This analysis did not delve into the uses of the bleed air, or the

cooling requirements for the turbine. An analysis is necessary to determine the impact of the aspiration on the cycle efficiency of the engine. Once the cycle efficiency is determined, the overall impact of the engine needs to be coupled with an airframe to determine the mission impact of the engine. While it is possible that the cycle efficiency may go down, it is very likely that the reduced weight and size of an aspirated engine would offset any increase in cycle inefficiency. It is important to remember that the entire system is the complete aircraft and not simply the compressor or engine.

Appendix A: MTFLOW code description an use

Code description

From Design And Analysis Of Axial Aspirated Compressor Stages by Ali A. Merchant, 30 June 1999 in fulfillment of the requirements for the degree of Doctor of Philosophy from the Department of Aeronautics and Astronautics at the Massachusetts Institute of Technology.

Section 4.4.2.1 Code Description

In MTFLO, only the momentum equations are discretized in a strong conservative form on a meridional streamline grid. The streamwise momentum equation has the form

$$dp + \rho q dq + \frac{\rho V_\theta}{r}[d(rV_\theta) - V_\theta dr] + pd(\Delta S) - pd(\Delta H_b) = 0 \qquad (4.21)$$

where q is the merdional velocity $\sqrt{V_x^2 + V_r^2}$ and the differentials $d()$ are taken along a streamline. The normal momentum is used to impose pressure continuity along neighbering streamlines. The stage work is defined as

$$\Delta H_b \equiv \int \Omega d(rV_\theta) \qquad (4.22)$$

where rV_θ is prescribed and Ω is non-zero for rotating blade rows. The entropy is defined as

$$S \equiv \ln\left[\frac{(h/h_{inl})^{\gamma/\gamma-1}}{P/P_{inl}}\right] \qquad (4.23)$$

so that $S_{inl} = ln(1) = 0$ by definition, and ΔS is the prescribed entropy variation along a streamline. The differential energy equation is not solved but instead the total enthalpy H is explicitly prescribed at every point in the flowfield using the relation

$$H = h_{inl} + \tfrac{1}{2}q_{inl}^2 + \Delta H_q + \Delta H_b \qquad (4.24)$$

where may be due to heat addition. The total enthalpy rise is related to the static enthalpy and all velocity components follows.

$$H = h + \tfrac{1}{2}V_z^2 + \tfrac{1}{2}V_r^2 + \tfrac{1}{2}V_\theta^2 = h + \tfrac{1}{2}q^2 + \tfrac{1}{2}V_\theta^2 \tag{4.25}$$

With these definitions, the streamwise momentum equation (4.21) above can be manipulated into an entropy-convection equation with the imposed source terms due to heat addition and adiabatic loss.

$$-pdS + pd(\Delta S) + \rho d(\Delta H_q) = 0 \tag{4.26}$$

Equation (4.26) can optionally replace the momentum equation (4.21) in all or part of the flowfield, and preferable since it eliminates the generation of spurious entropy due to numerical errors. Finally, continuity is enforced by prescribing equal mass fractions of the total mass flow in each streamtube. The meridional speed q can be solved from

$$q = \frac{\dot{m}}{\rho AB} \tag{4.27}$$

where A is the cross sectional thickness of the streamtube, and B is the blockage defined in (4.11) which acts to restrict the flow area.

The discrete equations described above are arranged in a form where the unknowns are the change in density and streamline positions, and the non-linear system is solved using a global Newton method. A particular advantage of this approach is that the streamline positions are simultaneously calculated as part of the solution and no explicit iteration is required to update the streamline positions as in traditional streamline curvature codes making MTFLOW computationally inexpensive and extremely robust.

4.4.2.2 Parameter and Geometry I/O

The geometry input requires the flowpath definition which includes profiles of the hub and casing. The meridional projection of all the blade rows in the flowpath are also required to determine the axial extent of the prescribed distributions. The wheel speed is specified for each blade row along with the number of blades per row. The circulation rv_θ, blockage B, and adiabatic loss ΔS are specified spanwise profiles along the trailing

edge of a blade row. The prescribed quantities, which are a function of the meridional blade geometry, are transferred on to the corresponding streamlines which interest the blade during the grid generation phase.

The geometric output from MTFLOW consist of streamline thickness and position in the meridional plane. A streamline, or group of streamlines, within specified axial limits, for example on either side of a blade row, are output in terms of total streamtube thickness $b(m')$, average and radial position $r(m')$ where m' is the meridional arc length along the streamtube. Radial profiles of flow conditions such as absolute and relative Mach numbers, flow angles, and wheel speed in the relative frame can also be extracted from any point in the flow field.
End of selection

Grid generation problems

The griding algorithm creates streamtubes through the geometry. Streamwise points along the streamtubes create the mesh. The spacing for these points is governed by the requirement that the lines are vertical, when viewed in cross section, for the entrance and the exit of the geometry. All streamtubes have the same number of streamwise points, and the spacing is determined by the curvature of the streamsurface. This griding scheme leads to sheared cells in areas of high curvature of the hub or tip geometry. Increasing the streamwise points to the maximum allowable by the code reduces the cell shearing. This cell shearing caused problems where the local mach number in the region of the cells was near unity. Decreasing the local mach in these areas solved the problem.

Another problem caused by the grid generation, was the positioning of the blades. For the purposes of the model, the blade leading edges were positioned to approach the curvature of the grid. This was necessary because the large grid shearing in some of these regions, along with the high enthalpy change in the blades, caused problems. The LE curvature allowed the changes in the flow due to the blade to be imparted in cells that were close in terms of streamwise positioning. If this was not done, the position of the LE varied by several streamwise cells from the hub to the tip. This curvature of the LE is a function of the grid generation, and not based on physical phenomenon. The actual positioning of the LE will be determined when blade shapes are designed for the various blades. For the purpose of determining the solidity, and for graphical representation in this report, the axial position of the blades LE was not varied from hub to tip.

Appendix B: Data files for MTSOL and MTSET

Geometry file: Blade.cr3

```
Dec92rotors
-0.9 1.67 0     0
      -1.000    0.000
      -0.600    0.001
      -0.350    0.019
      -0.280    0.063
      -0.227    0.117
      -0.173    0.178
      -0.118    0.235
      -0.051    0.293
      0.000     0.335
      0.070     0.395
      0.135     0.450
      0.225     0.528
      0.269     0.566
      0.293     0.584
      0.322     0.608
      0.372     0.646
      0.426     0.682
      0.542     0.742
      0.592     0.764
      0.889     0.856
      0.921     0.857
      1.112     0.855
      1.306     0.750
      1.442     0.765
      1.470     0.782
      1.570     0.797
      1.580     0.797
      1.590     0.797
      1.620     0.797
      1.650     0.797
      1.700     0.797
      999.000   999.000
      -1.000    0.920
      -0.717    0.920
      -0.616    0.923
      -0.503    0.931
      -0.437    0.942
      -0.379    0.954
      -0.341    0.969
      -0.299    0.984
      -0.251    0.992
      -0.200    1.000
```

```
-0.100     1.000
-0.050     1.000
0.000      1.000
0.266      0.980
0.382      0.967
0.592      0.966
0.709      0.961
0.885      0.943
0.958      0.936
1.112      0.926
1.339      0.839
1.442      0.836
1.470      0.836
1.567      0.832
1.650      0.832
1.700      0.832
```

Blade file: stack.cr3

```
      Stack Definition

      Rle    Rte    Xle    Xte    Loss         THK    RVT

      25     -1.34352     1
      0.170 0.250 0.000 0.268 -0.100       0.000 -0.880
      0.333 0.567 0.000 0.268 -0.100       0.000 -0.880
      0.667 0.749 0.000 0.268 -0.110       0.000 -0.890
      0.745 0.800 0.000 0.268 -0.110       0.000 -0.890
      1.000 0.980 0.000 0.268 -0.120       0.000 -0.900
      1.360 1.286 0.000 0.268 -0.120       0.000 -0.900
999
      25     0      1
      0.485 0.608 0.309 0.592 -0.050       0.000 0.733
      0.611 0.764 0.322 0.592 -0.040       0.000 0.733
      0.845 0.887 0.361 0.592 -0.040       0.000 0.720
      0.965 0.950 0.382 0.592 -0.050       0.000 0.710
      1.255 1.294 0.380 0.592 -0.060       0.000 0.710
999
      87     1.56180993   1
      0.752 0.799 0.603 0.889 -0.070       0.000 1.200
      0.783 0.819 0.619 0.889 -0.100       0.000 1.200
      0.835 0.852 0.634 0.889 -0.100       0.000 1.200
      0.887 0.886 0.665 0.889 -0.160       0.000 1.200
      0.941 0.920 0.695 0.889 -0.170       0.000 1.200
      0.979 0.944 0.713 0.889 -0.190       0.000 1.200
999
      65     0      1
      0.780 0.823 0.921 1.112 -0.050       0.000 -0.606
      0.806 0.837 0.924 1.112 -0.050       0.000 -0.606
      0.849 0.860 0.929 1.112 -0.050       0.000 -0.606
      0.891 0.882 0.960 1.112 -0.050       0.000 -0.606
      0.935 0.906 0.988 1.112 -0.050       0.000 -0.606
      0.966 0.923 0.992 1.112 -0.050       0.000 -0.606
999
```

```
      65    -1.052      1
      0.745 0.798 1.310 1.442 -0.050      0.000 -1.500
      0.760 0.802 1.316 1.442 -0.050      0.000 -1.500
      0.786 0.809 1.322 1.442 -0.050      0.000 -1.500
      0.812 0.815 1.327 1.442 -0.050      0.000 -1.500
      0.838 0.822 1.333 1.442 -0.050      0.000 -1.500
      0.857 0.827 1.341 1.442 -0.050      0.000 -1.500
999
      65    0     1
      0.768 0.800 1.470 1.568 -0.050      0.000 1.100
      0.802 0.802 1.477 1.568 -0.050      0.000 1.100
      0.809 0.805 1.482 1.568 -0.050      0.000 1.100
      0.816 0.807 1.486 1.568 -0.050      0.000 1.100
      0.822 0.810 1.491 1.568 -0.050      0.000 1.100
      0.837 0.811 1.494 1.568 -0.050      0.000 1.100
```

References

[1] Merchant, A. A. "Design And Analysis of Axial Aspirated Compressor Stages." Doctoral Thesis, Massachusetts Institute of Technology, 1999.

[2] Merchant, A.A., 1999

[3] Merchant, A.A., 1999

[4] Merchant, A.A., 1999

[5] Merchant, A.A., 1999

[6] Merchant, A.A., 1999

[7] Johnsen, I.A., and Bullock, R.O., (eds), *Aerodynamic design of axial flow compressors*, NASA SP-36 U.S. Printing office, Washington, 1972

[8] Merchant, A.A., 1999

[9] Merchant, A.A., 1999

[10] Merchant, A.A., 1999

[11] Drela, M., "A users guide to MTFLOW 1.2", MIT Fluid Dynamics Research Laboratory, Unpublished 1997

[12] J.H. Horlock, *Axial Flow Turbines*, Robert E. Kreiger publishing Co., Melbourne FL, 1973

[13] J.L. Kerrebrock, *Aircraft engines and Gas Turbines*, 2nd ed. The MIT Press, Cambridge MA, 1992